MARINE MAMMAL SCIENCE, 23(1): 94–109 (January 2007)

DOI: 10.1111/j.1748-7692.2006.00094.x

# TURNING MANEUVERS IN STELLER SEA LIONS (*EUMATOPIAS JUBATUS*)

O. CHENEVAL
R. W. BLAKE[1]
A. W. TRITES
K. H. S. CHAN
Department of Zoology,
University of British Columbia,
Vancouver, British Columbia,
Canada V6T 1Z4, Canada
E-mail: blake@zoology.ubc.ca

## ABSTRACT

Steller sea lions are highly maneuverable marine mammals (expressed as minimum turning radius). Video recordings of turns ($n = 195$) are analyzed from kinematic measurements for three captive animals. Speed-time plots of 180° turns have a typical "V-shape." The sea lions decelerated during the first half of the turn, reached a minimum speed in the middle of the curved trajectory and reaccelerated by adduction of the pectoral flippers. The initial deceleration was greater than that for passive gliding due to pectoral flipper braking and/or change in body contour from a stiff, straight streamlined form. Centripetal force and thrust were determined from the body acceleration. Most thrust was produced during the power phase of the pectoral flipper stroke cycle. Contrary to previous findings on otariids, little or no thrust was generated during initial abduction of the pectoral flippers and during the final drag-based paddling phase of the stroke cycle. Peak thrust force at the center of gravity occurs halfway through the power phase and the centripetal force is maximal at the beginning of the power stroke. Performance is modulated by changes in the duration and intensity of movements without changing their sequence. Turning radius, maximum velocity, maximum acceleration and turning duration were 0.3 body lengths, 3.5 m/s, 5 m/s$^2$, and 1.6 s, respectively. The relative maneuverability based on velocity and length specific minimum turning radius is comparable to other otariids, superior to cetaceans but inferior to many fish.

Key words: Steller sea lion, *Eumetopias jubatus*, kinematics, turning, speed, acceleration, forces.

Many studies on the locomotion of aquatic animals have focused on steady and fast-start swimming performance, and maneuverability has been less well studied (see Blake 2004 for a review). Animals rarely swim in a steady rectilinear fashion,

[1] Author to whom correspondence should be addressed.

especially in structurally complex habitats. Marine mammals and fish in coastal environments maneuver and adjust their trajectories in the face of destabilizing currents and obstacles. Maneuverability is also a key component of predator–prey interactions (Howland 1974) in the aquatic environment where predators are often substantially larger and faster than their prey. Previous swimming studies on marine mammals have focused on drag, functional design, and maximum forward speed (*e.g.*, English 1976; Williams and Kooyman 1985; Feldkamp 1987a,b; Fish *et al*. 1988; Ponganis *et al*. 1990; Fish 1993; Stelle *et al*. 2000). Weihs (2002) and Fish (2002) discuss the direct performance conflicts between maneuverability and stability in aquatic locomotion in the context of functional design. A maneuver is a change of trajectory and/or velocity caused by a linear and/or rotational acceleration and may be viewed as a controlled instability during which the sum of all forces and moments acting at the center of gravity of the animal does not equal zero. Unbalanced forces are promoted by body flexibility and highly mobile control surfaces positioned close to the center of gravity (Fish 1997, Fish *et al*. 2003). In contrast, adaptations for steady, rectilinear swimming include a streamlined rigid body and limited mobility of control surfaces (Blake *et al*. 1995). Maneuvering is energetically more costly than steady swimming (Webb 1991, Hughes and Kelly 1996).

Turns involve rotation and translation but certain fish propelled by median and/or paired fins can generate rotation at zero forward speed (*e.g.*, boxfishes; Blake 1977, Walker 2000). Bottlenose dolphins (*Tursiops truncates*) exhibit a "pinwheel" turning technique that minimizes turning radius and maximizes turning rate by transforming forward speed into rotational speed (Nowacek 2002, Maresh *et al*. 2004). Both turning components are typically maximized in predator–prey interactions (*i.e.*, a tight turn with a high translation speed, Howland 1974). The turning dynamics of Steller sea lions is an important ingredient in understanding the predator–prey relations of this endangered species that may be subject to acute nutritional stress (Trites and Donnelly 2003).

Turning dynamics, pectoral flipper kinematics, turning radius, and rates have been described for California sea lions *Zalophus californias* (English 1976; Godfrey 1985; Feldkamp 1987a,b; Ponganis *et al*. 1990; Fish *et al*. 2003). However, these studies focus on general descriptions of turning, specific turning radii, and turning rate, and little is known about the performance and kinematics of other otariids. We filmed three Steller sea lions *Eumatopias jubatus* performing 180° turns. In addition to descriptive kinematics and performance measurements, we analyze the principle components of force generated in relation to body and flipper movements throughout turning maneuvers. Furthermore, the turning trajectory of the animals is compared to the predictions of a hydromechanical model of passive turning when gliding (Blake and Chan, in press) to assess the role of control surfaces during maneuvers. The turning performance of Steller sea lions is compared to that of other otariids, cetaceans, and fish.

## METHODS

Morphological measurements (weight, length, and girth) were made on three female Steller sea lions at the Vancouver Aquarium Marine Science Center (Vancouver, British Columbia, Canada) from August 15th to December 3rd, 2003. Two 3-yr-old juvenile females (F00YA and F00TS, referred to as SL1 and SL2, respectively) and a 6-yr-old adult female (F97HA, referred to as SL3) were kept in an outdoor facility with constant access to ambient, filtered seawater (Rosen and Trites 2004). Tests

were performed in a 19-m long, 5-m deep pool with rock and wooden haul-out areas. During the course of the study, the animals were fed Pacific herring. Experiments occurred over 50 d, 29 d, and 11 d for SL1, SL2, and SL3, respectively. Measurements were made on each animal prior to filming. Total length was measured from the tip of the nose to the tip of the hind flippers and standard length was taken from the tip of the nose to the base of the tail.

Body volume and wetted surface area were calculated as a succession of truncated cones. Eight girth measurements were taken at known intervals along the body (the ears, the neck, directly in front of the pectoral flippers, directly behind the pectoral flippers, two places along the trunk region between flippers and hips, the hips, and the position where the body and the hind flippers meet) each forming the base of a truncated cone. The animals were weighed daily (GSE scale, Model 350, SPX Corporation, scale accuracy $\pm$ 0.1 kg). Body density was obtained by dividing the calculated volume (including the volume of the flippers) by the mass of the animal. The location of the center of gravity was determined using the method of Domning and de Buffrénil (1991).

Flipper projected surface area, length, and width were obtained from scaled still photographs (PC with Scion Image software, Beta version 4.0.2 Scion Corporation). Thickness measurements were made with a spring-joint caliper (measurement accuracy: $\pm$ 0.5 mm) at 13 locations along the pectoral flipper (4 along the leading edge, 4 along the midline, 4 along the trailing edge and 1 at the tip, all measurements were approximately 15 cm apart). Pectoral and flipper aspect ratios (ARs) were calculated as $AR = (length)^2/(projected\ surface\ area)$. The volumes of pectoral and pelvic flippers were calculated from these measurements. These values were used in the calculation of the total volume of the animal.

Animal weight fluctuated over the course of the study (maximum mass change: 7.6%, 5.8%, and 5.6% for SL1, SL2, and SL3, respectively; Cheneval 2005). The highest values of the range were used to determine the morphological measurements directly affected by mass variations (Table 1). Body length showed less variation (average increase: 0.7%, range: 0.2%–1.4%). With the exception of the hip area (where the body is slightly dorso-ventrally compressed), the body of the Steller sea lions has a rounded cross-section when in the water and a circular cross-section was assumed in all calculations of volume, wetted surface area, and frontal surface area. Pectoral and pelvic flippers represented 56% and 44% of the total projected flipper area and the mean ARs of the pectoral and pelvic flippers were 3.2 and 2.4, respectively.

The training method (positive reinforcement) was similar to that of Fish *et al*. (2003). The sea lions were trained to swim back and forth between two trainers positioned at opposite ends of the test pool. As the animal approached Trainer 2, Trainer 1 would perform a recall signal (hit the surface of the water with a target pole) after which the animal executes an 180° turn (Fig. 1). After preliminary trials, the distance between the two trainers was reduced to 9–12 m by having one trainer sitting in a kayak 3–5 m away from the field of view of a video camera. The animal had room for at least one complete flipper stroke before entering the field of view of the camera.

The turns were filmed with a digital video camera (Canon GL-2, 60 Hz, zoom setting attached equivalent to a 39.5 mm opening on a 35-mm focal length corresponding to a diagonal angle of 57.42° formed at the apex of the triangle defined by two opposite corners of the field of view and the focal point of the camera) 5 m above and normal to the water surface. A circular polarizing filter (Hoya circular polarizing

*Table 1.* Morphological data on three female Steller sea lions.

| Animal | | 1 | 2 | 3 |
|---|---|---|---|---|
| Age | [yr] | 3 | 3 | 6 |
| Body mass | [kg] | 124.2 ± 4.8 | 144.2 ± 4.3 | 144.6 ± 4.1 |
| Total length | [m] | 2.27 ± 0.02 | 2.29 ± 0.02 | 2.26 ± 0.02 |
| Standard length (L) | [m] | 1.83 ± 0.02 | 1.87 ± 0.02 | 1.92 ± 0.02 |
| Frontal surface area | [$m^2$] | 0.149 ± 0.004 | 0.156 ± 0.004 | 0.167 ± 0.004 |
| Total wetted surface area | [$m^2$] | 2.391 ± 0.066 | 2.551 ± 0.061 | 2.481 ± 0.059 |
| Volume | [l] | 137.3 ± 10.4 | 154.7 ± 8.9 | 150.8 ± 8.4 |
| Fineness ratio | — | 5.2 ± 0.2 | 5.1 ± 0.2 | 4.9 ± 0.2 |
| Position of max thickness | [% of L] | 44.3 | 42.8 | 45.8 |
| Position of center of gravity | [% of L] | 57.4 | 55.6 | 51.6 |
| Pectoral flipper area | [$m^2$] | 0.104 | 0.115 | 0.107 |
| Pectoral length | [m] | 0.58 | 0.60 | 0.60 |
| Pectoral max width | [m] | 0.23 | 0.24 | 0.24 |
| Pectoral aspect ratio | — | 3.23 | 3.13 | 3.32 |
| Pelvic flipper area | [$m^2$] | 0.085 | 0.082 | 0.092 |
| Pelvic length | [m] | 0.45 | 0.46 | 0.46 |
| Pelvic max width | [m] | 0.28 | 0.25 | 0.29 |
| Pelvic aspect ratio | — | 2.38 | 2.53 | 2.26 |
| Total flipper area | [$m^2$] | 0.378 | 0.394 | 0.396 |

filter, 58 mm, pitch: 0.75) was used to reduce flares and surface reflections. A clear Plexiglass sheet (dimensions: 2.61 m × 1.98 m) floated on the water surface in the center of the field of view of the camera to eliminate distortions produced by surface waves. Only turns that occurred directly under the Plexiglass sheet were analyzed.

Temporary marks (2.5 cm in diameter, oil-based pastel crayons), which could be tracked on the video images, were made on the fur of the animals. Points were placed on the shoulder blades (shoulder), the center of gravity of the animal stretched straight with its pectoral flipper tucked in (CG), and on the hipbone (hips). Each marking was drawn three times around the animals' girth: on the left side, right side, and along the backbone. The motion of the animals was not limited vertically. The turning radius as seen in two dimensions by the overhead camera was corrected for depth using a visual scale (a 2 m long ruler with 10 cm increments, $Depth = -0.056 \times Size\ on\ screen\ in\ pixels + 8.63$).

Turning radii, instantaneous speed at the start and end of a turn, average speed, acceleration, and duration of the maneuver were measured from the scaled video clips using Lenox Softworks' Videopoint 2.5. All turns were referenced to an on-screen origin. The positions of the three lateral dots (shoulder, CG, and hips) were tracked at a sampling rate of 30 Hz. Instantaneous speed ($U_n$) was calculated as:

$$U_n = \frac{P_{n+1} - P_{n-1}}{t_{n+1} - t_{n-1}}, \tag{1}$$

where $P_{n+1}$ and $P_{n-1}$ are the positions of the points, and $t_{n+1}$ and $t_{n-1}$ is the time code of the points directly after and before point $n$. The speed profile was obtained by plotting instantaneous velocities over time. To correct any difference in depth before and after the maneuver, the speed calculation was modified as follows:

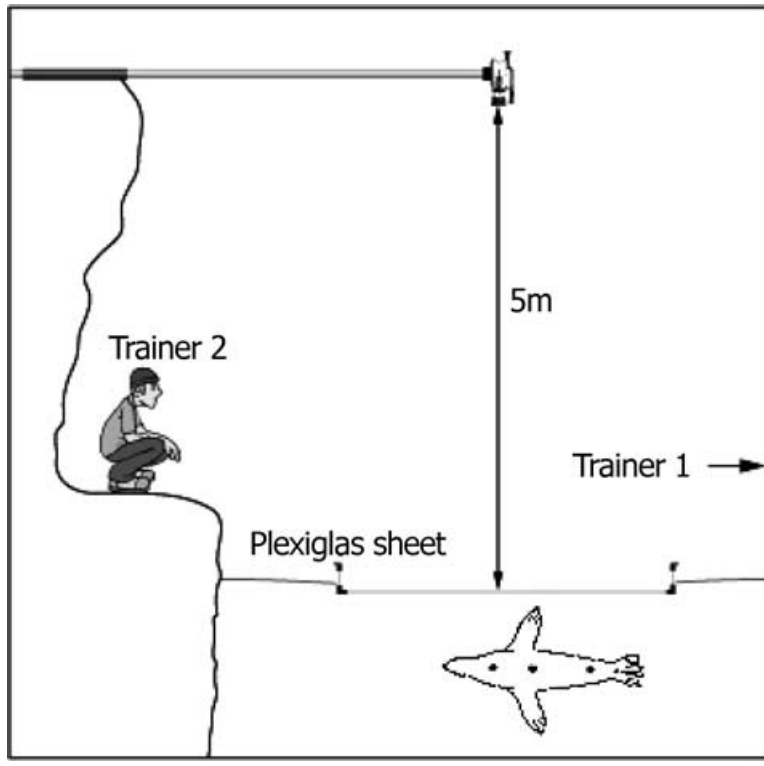


*Figure 1.* Schematic of the experimental setup.

$$U_{n(\text{corrected})} = \frac{U_n}{\cos \alpha}, \tag{2}$$

where $\alpha$ is the angle between the center line of the animal and the camera.

Turning radius ($R$) was calculated by fitting a half circle to the curved part of the trajectories of the shoulder, the center of gravity, and the hip (*i.e.*, three turning radii were obtained per maneuver). The trajectories obtained in Videopoint 2.5 were imported into S-PLUS 6.1, where the least-squared regressions were performed. Once $R$ was measured, the real turning radius was obtained by taking the depth difference into account:

$$R_{\text{real}} = \sqrt{(R_{\text{measured}})^2 + \left(\frac{\Delta D}{2}\right)^2}, \tag{3}$$

where $\Delta D$ is the difference of depth between the entrance and exit of a maneuver. The speeds at the beginning and at the end of the turn were defined as the instantaneous speed of the animal just before initiating the maneuver and when the body midline was straight with the pectoral flippers adducted, respectively. The time duration of a maneuver was defined as the time elapsed between entering and exiting the turn.

We present turning time as a percentage of the turning bout and present the events with respect to percent of the cycle.

Acceleration measurement (and therefore force) is sensitive to the position of the markers on each frame. A smooth cubic spline function was fitted to the position-time data. Calculated speed and acceleration are

$$U_p = \frac{P_{p+1} - P_{p-1}}{t_{p+1} - t_{p-1}} \qquad a_p = \frac{U_{p+1} - U_{p-1}}{t_{p+1} - t_{p-1}}, \tag{4}$$

where $U_p$ is the instantaneous speed of point $p$ (m/s), $P_{p+1}$, and $P_{p-1}$ are the positions (m), $t_{p+1}$, and $t_{p-1}$ are the time codes (s) of the points directly after and before point $p$, $a_p$ is the instantaneous resultant acceleration of point $p$ (m/s$^2$) and $U_{p+1}$ and $U_{p-1}$ are the instantaneous velocities (m/s). This process provided the $X$ and $Y$ components of the acceleration vector. One component of the acceleration vector was therefore parallel to the instantaneous velocity vector (tangential acceleration $a_t$) and one component was perpendicular to the velocity vector (normal acceleration $a_n$).

ANOVA was performed on entering speed, exiting speed, turn duration, deceleration, acceleration, and turning radius to determine interanimal differences (SPSS 8.0) at $\alpha = 0.05$.

## Results and Discussion

All turns ($n = 419$) were partially unpowered maneuvers performed with a nonzero initial speed. A total of 195 (64 turns for SL1, 70 for SL2, and 61 for SL3) occurred directly under the Plexiglass sheet and were kept for further analysis. In all turns analyzed, the three animals used the same general turning technique similar to that of the California sea lion (Fish *et al*. 2003). Figure 2 shows a representative sequence of turning movements. The head is oriented toward the inside of the turn and the pectoral flippers are abducted (Fig. 2, 1a). The body starts flexing dorsally (Fig. 2, 1b); the abduction of the pectoral flippers ends and the interdigital web of the pelvic flippers starts to open (Fig. 2, 1c). Maximal dorsal arching occurs when the digits of the pelvic flipper open (Fig. 2, 2). The pectoral flippers are adducted with the interdigital web maximally spread (Fig. 2, 3a). As the body regains a straight position, the pectoral flippers reach the end of the power stroke (paddle phase) and the pelvic flippers return to their gliding position (Fig. 2, 3b). Performance variation is modulated by varying the duration and/or intensity of each movement of the three turn phases (Fig. 2), but the overall sequence of the movements is consistent.

Turning radius, speed, normal and tangential acceleration, and turn duration are shown in Table 2. Turns were performed in 1.65 ± 0.17 s (mean ± 2 SE), 1.74 ± 0.20 s, and 1.32 ± 0.13 s for SL1, SL2, and SL3, respectively. Turning duration was significantly different among all animals, and interanimal variations were observed on all measured parameters except for the deceleration of the CG ($P < 0.05$; Table 2). Turning radius, maximum velocity, maximum acceleration, in speed, out speed, and rolling time were 0.3 BL, 3.5 m/s, 5 m/s$^2$, 2.8 m/s, 3.4 m/s, and 1.6 s, respectively.

Instantaneous speed plotted against time gives a typical "V-shaped" curve in all turns (Fig. 3). Gliding speed decreased prior to the first movement of the head into the turn coincident with the start of pectoral flipper abduction, and this occurred during the interval of $t$ = 0–0.8 s at 0%–50% of the turning cycle. Acceleration begins prior to the onset of flipper adduction. The turn ends with the paddle phase of

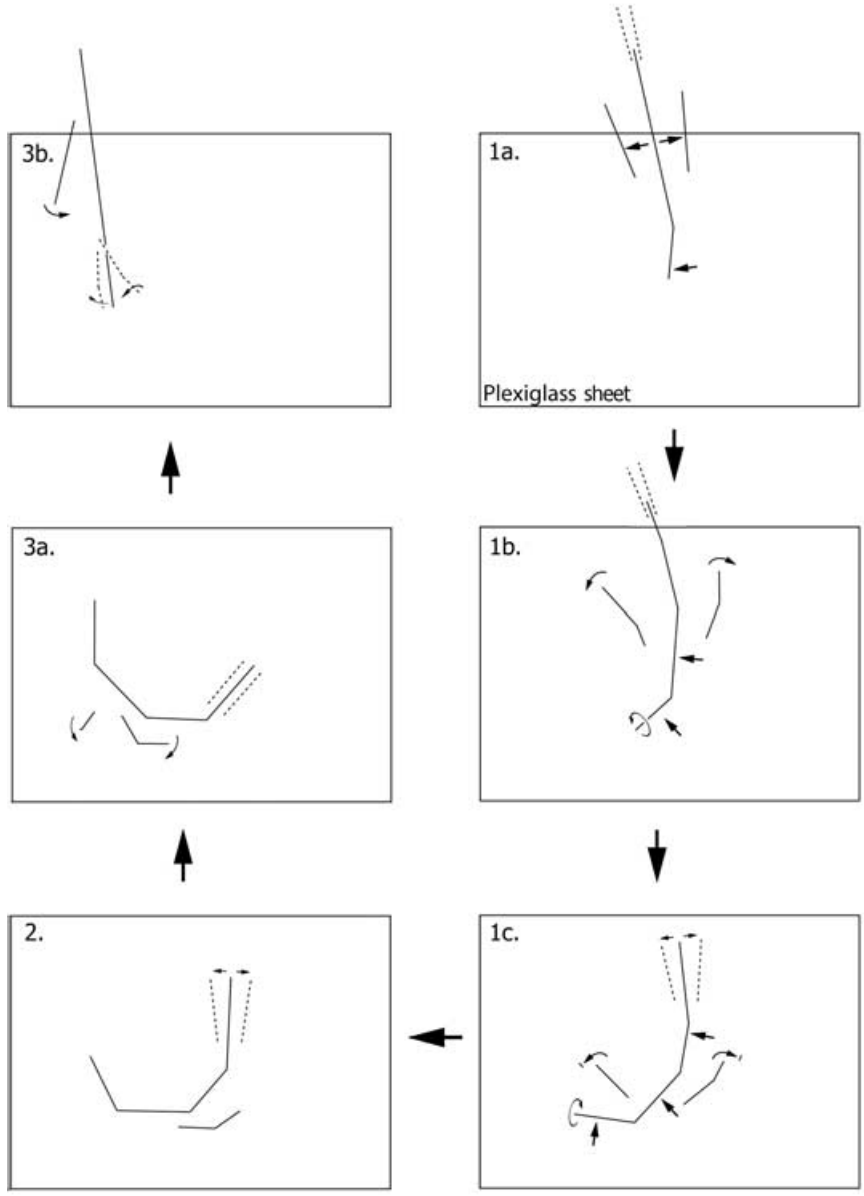


*Figure 2.* Sequence of movements based on a representative turn performed by SL3. Arrows indicate the principal movements of the animal in each frame.

the flipper stroke. Each body marker (shoulders, CG, hips) follows a slightly different trajectory, which is reflected in the different speed profiles (Table 2; Fig. 3). Minimum speed occurred just before the middle of the 180° trajectory at about 50% of the cycle where $t \approx 0.8$ s (Fig. 3). The speed trajectory of the shoulders was followed by the

*Table 2.* Mean kinetic parameters for three Steller sea lions. The gray tones (white, gray, dark gray) represent a significant difference between each animal at $\alpha = 0.05$.

| Animal | 1 | 2 | 3 |
|---|---|---|---|
| In speed [m/s] | 2.69 | 2.93 | 2.92 |
| Out speed [m/s] | 3.22 | 3.08 | 3.77 |
| Rolling time [s] | 0.76 | 0.74 | 0.64 |
| Turn duration [s] | 1.65 | 1.74 | 1.32 |
| Turning radii [BL] | | | |
| Shoulders | 0.32 | 0.31 | 0.26 |
| Center of gravity | 0.32 | 0.30 | 0.27 |
| Hips | 0.33 | 0.33 | 0.26 |
| Deceleration [m/s$^2$] | | | |
| Shoulders | −1.75 | −2.40 | −2.43 |
| Center of gravity | −1.31 | −1.65 | −1.48 |
| Hips | −1.20 | −1.84 | −1.89 |
| Acceleration [m/s$^2$] | | | |
| Shoulders | 2.50 | 3.39 | 3.96 |
| Center of gravity | 2.70 | 3.01 | 3.29 |
| Hips | 4.11 | 3.86 | 7.12 |

CG and the hips. As the animal exited the turn after $t = 0.8$ s, the shoulders and the CG reaccelerated at a similar rate, and the acceleration of the hips was considerably higher (Fig. 3). The minimum speed of each body marker was reached before the middle of their respective curved trajectories (dotted lines, Fig. 3). For the shoulders and the CG, the minimum was reached before the start of the power phase. The hips reached their minimum speed later, approximately at the start of the power phase. The minimum speed of the shoulders and the center of gravity was followed by a bout of constant or even slightly increasing speed (*i.e.*, a "flat" minimum) during which the pectoral flippers were abducted and motionless. As the animal arches dorsally, the hips move outside of the turn and their trajectory departs from the trajectory of the two other markers. This is a result of the rotational moment created by the displacement of the head inside the turn. As the body regains a straight position at the end of the turn near the completion of the turning cycle, the trajectory of the hips crossed the other two tracks (Fig. 3) and hips therefore accelerated faster than the shoulders and CG. The reacceleration phase occurred at $t = 0.8$–$1.4$ s.

The tangential and normal acceleration (parallel and perpendicular to the velocity vector, respectively) are shown in Figure 4 for each body section. The tangential acceleration closely followed the variations in the speed profile (Figs. 3 and 4). When gliding, the tangential acceleration of the shoulders and CG reached a minimum approximately when the pectoral flippers were fully adducted. As speed increased, the tangential acceleration became positive before returning to zero as the animal glided out of the turn. The deceleration of the hips corresponded to the movements of the pelvic flippers, remaining negative through the first half of the turn, reaccelerating abruptly as the hips' trajectory "cut through" those of the other body sections as the animal straightened. The maximum tangential acceleration of the hips was reached just before the end of the pectoral flipper power stroke phase.

Normal acceleration was greater than and preceded the tangential acceleration (Figs. 3 and 4). During the linear glide preceding the turn, the normal acceleration of

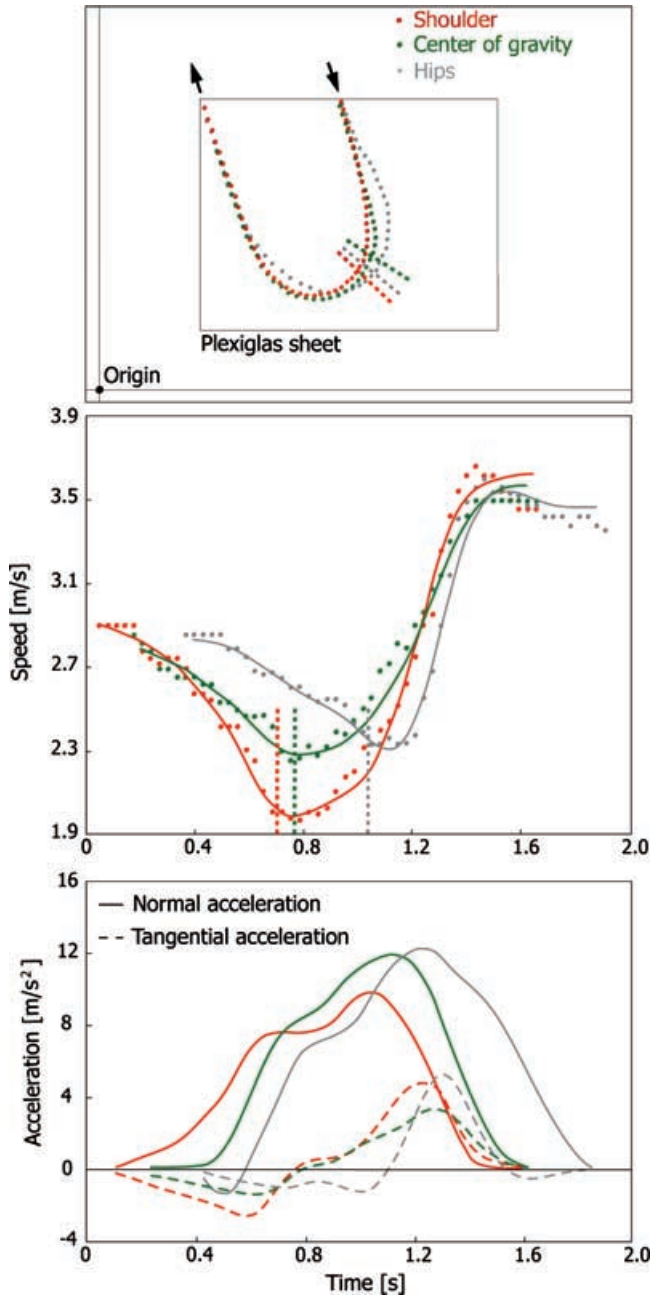


*Figure 3.* Typical trajectory and speed profile of the shoulder, center of gravity, and hips of a Steller sea lion performing a 180° turn. The minimum speed is represented as vertical dotted lines. Tangential (dashed lines) and normal acceleration (solid lines) of the shoulder, the center of gravity, and hips are shown as a function of time.

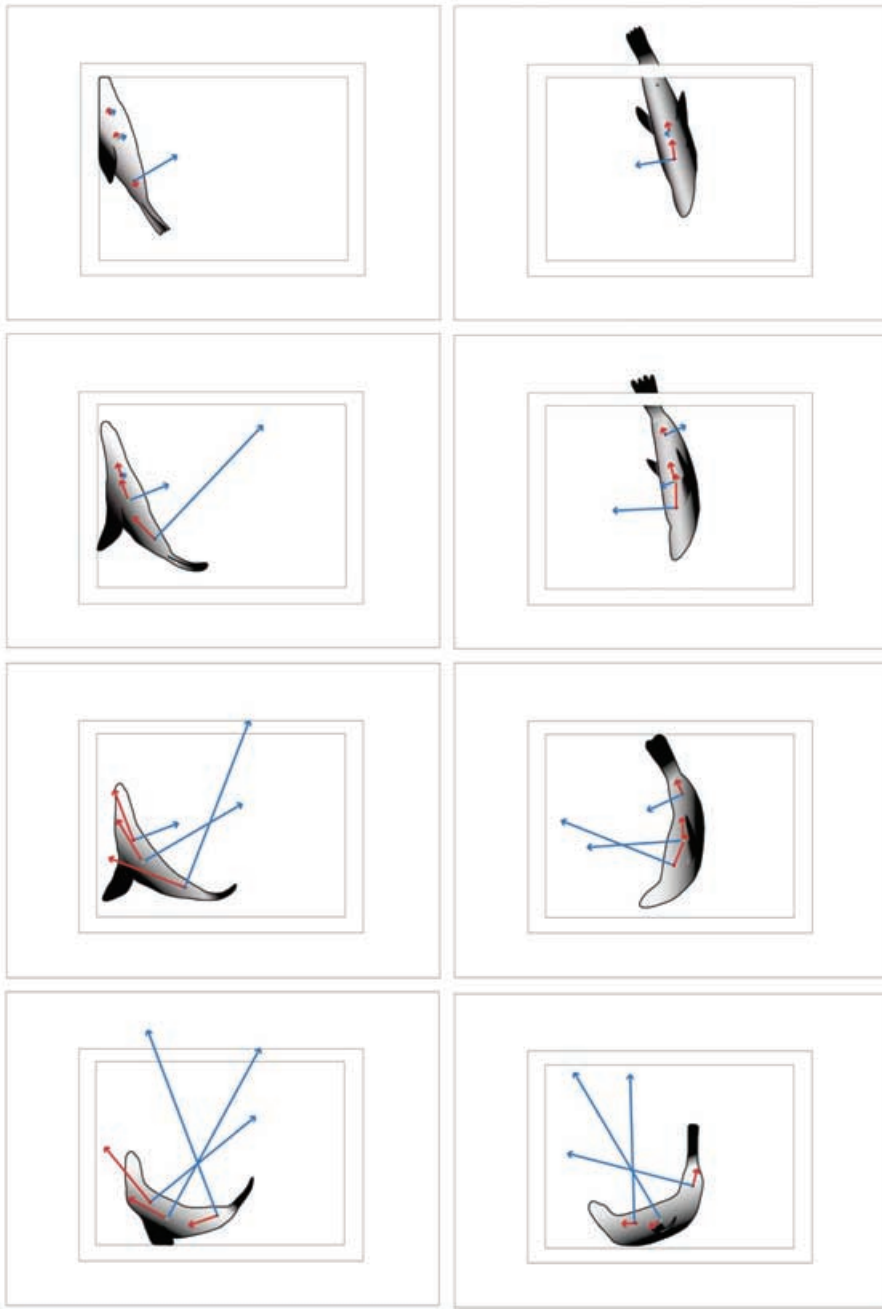

*Figure 4.* Normal and tangential acceleration throughout a 180° turn performed by a Steller sea lion. Blue and red arrows indicate normal acceleration and tangential acceleration, respectively.

the shoulder and center of gravity was close to zero and increased when the animal oriented its head into the turn, reaching a maximum just after the start of the pectoral flipper power stroke phase. The normal acceleration of the hips coincided with dorsal flexion of the body and reached its maximum halfway through the pectoral flipper power phase returning to zero as the body regained a straight position.

The drag difference in a passive glide and turn that involves both body and flipper movements is shown for a fast and a slow 180° turn (Fig. 5). Lateral body flexure and flipper deployment change the streamlining of the animal relative to the incoming flow, increasing the drag coefficient by about three times that predicted for a linear glide where the pectoral flippers lie along the animal's ventral-lateral surface (Stelle *et al*. 2000). The pectoral flippers are positioned close to the center of gravity and act as independent deflectors and hydrofoils generating lift forces toward the inside of the turn changing the trajectory of the center of gravity. The bilateral pectoral flipper stroke cycle is made up of a lift-based recovery phase and a power phase based on lift followed by drag-based paddling as in the California sea lion (Feldkamp 1987a). The recovery and power phases occur during the first and second half of the turn, respectively. Pelvic flippers also play an active role in turning by resisting outward slip of the pelvic area.

For California sea lions, the total flipper area is 58% less than that of our Steller sea lions (total flipper area: 0.23 $m^2$ [Fish *et al*. 2003] and 0.389 $m^2$ for the California and the Steller sea lions, respectively) of comparable size (L = 1.9 m, mass = 138 kg for the male California, and L = 1.9 m, mass = 138 kg on average for the Steller sea lions) reflecting the early development of the flippers in Steller sea lions preceding bodily growth. The mass variation during the course of the experiments (of the order of 5%) for the three animals studied here is not a significant source of error. Steller sea lions are the largest otariids with males and females reaching up to 1,120 kg and 350 kg, respectively (Loughlin *et al*. 1987, Winship *et al*. 2001). California sea lions grow up to a maximum of 390 kg and 110 kg for males and females, respectively (Riedman 1990). The difference in flipper area between the Steller and California sea lions should translate to relatively higher lift forces and a more sudden change of trajectory for Steller sea lions. Also, large flippers moved slowly produce thrust more efficiently than small flippers moved rapidly (English 1976). However, lift increases with AR, and the AR of the pectoral flippers of California sea lions (4.2) is greater than that of Steller sea lions (3.2); The turning performance (based on velocity and minimum turning radius) of small Steller sea lions (Figs. 6 and 7) and adult California sea lions is comparable (Fish *et al*. 2003; Fig. 7). The minimum turning radii are 0.12 bodylengths (BL) and 0.14 BL for California and Steller sea lions, respectively. Maximum velocity was 3.58 m/s for California sea lions and 3.5 m/s for Steller sea lions. Although California and Steller sea lions have comparable turning radii, California sea lions turn at slower velocities (Fig. 7). However, sample sizes are small ($n = 2$ for California sea lions, Fish *et al*. 2003; $n = 3$ for Steller sea lions, this study) and there may differences of motivation to perform in the two species. Fish *et al*. (2003) noted that the attitude of the flippers in the California sea lion is highly variable and that the body of the animal is very flexible in the dorso-ventral plane. This combination of highly mobile control surfaces and body flexibility provides both species with an impressive array of maneuvering capabilities within one stereotypic turning pattern.

Steller sea lions and (otariids in general) are opportunistic predators that forage on a wide variety of prey species (*e.g.*, gadids, salmonids, small schooling fish, flatfish,

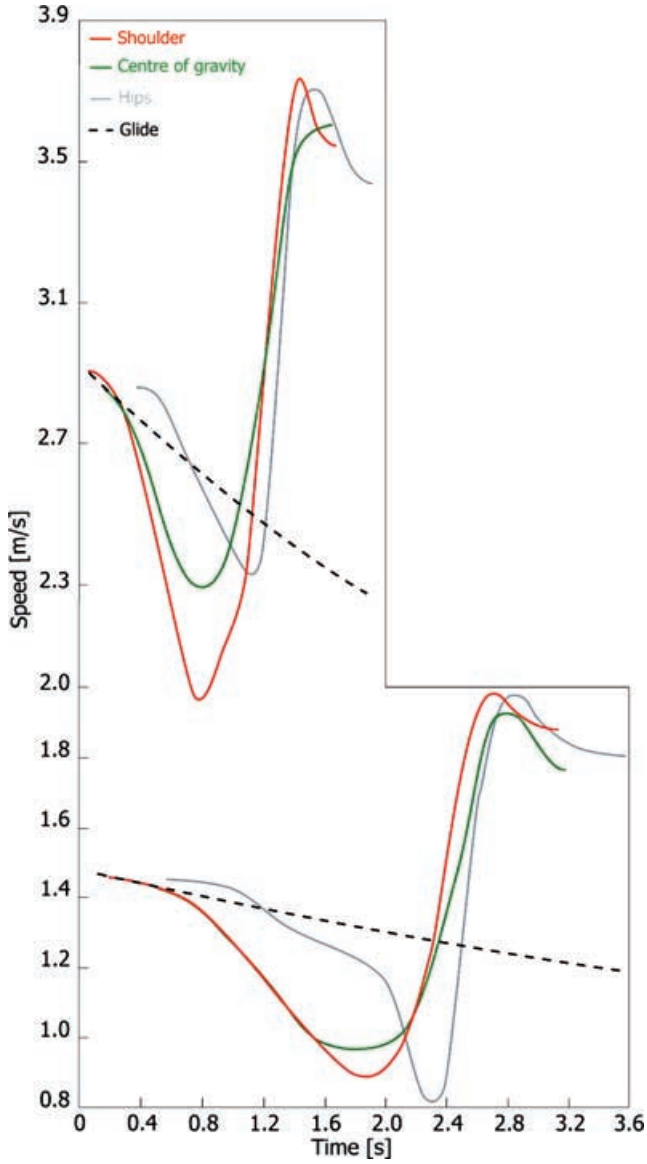


*Figure 5.* Comparison of the speed profiles of the shoulder, center of gravity, and hips markers of a Steller sea lion performing a fast and a slow 180° turn. The dashed black lines represent the theoretical speed of a passive glide. (Blake and Chan 2006)

and cephalopods; Riedman 1990, Merrick *et al*. 1997, Sinclair and Zeppelin 2002) where frequent, rapid maneuvers are employed. Predatory success depends on coming within striking distance from prey prior to a rapid neck extension followed by a bite. Their predators (*e.g.*, killer whales [*Orcinus orca*] and great white sharks [*Carcharodon carcharias*]) swim faster than they do (Riedman 1990), and to escape they must "out maneuver" them and/or escape to a terrestrial refuge.

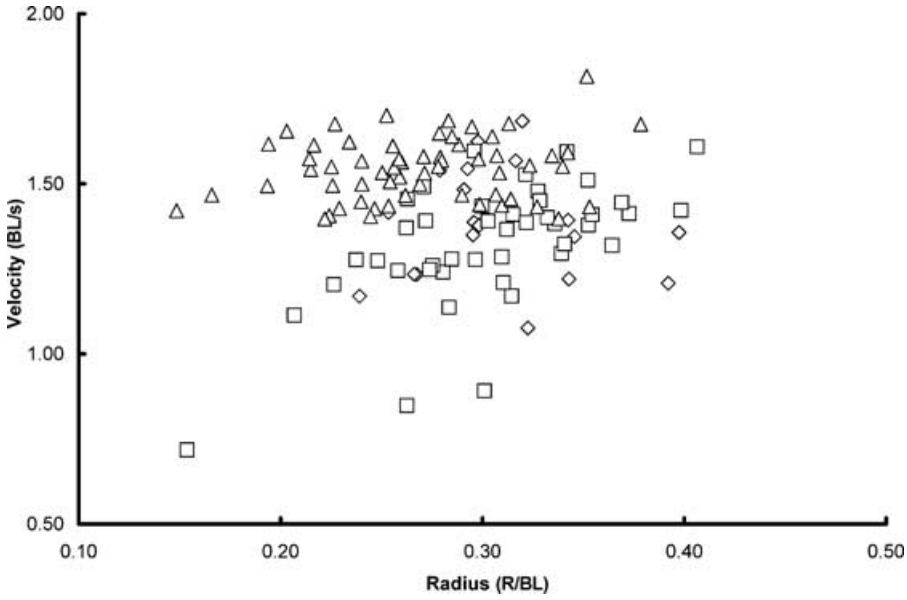


*Figure 6.* Standardized turning speed (body length/s) *versus* normalized turning radius (turning radius/body length) of Steller sea lions SL1 (diamond; $n = 19$), SL2 (square; $n = 43$), and SL3 (triangle; $n = 60$).

High turning performance is desirable for both predators and prey (Howland 1974). Turning radius and BL are linear related in aquatic vertebrates (*e.g.*, Domenici and Blake 1993, Domenici *et al*. 2004). Because BL is cubically proportional to body mass, turning radius should scale with body mass to the power of 1/3. The empirical fit of a log–log plot of turning radius versus body mass for fish, sea lions, and cetaceans has a slope of 0.37, close to the expected value (Blake and Chan 2006). This implies that maneuverability decreases with BL as minimum turning radii and maximum turning rates increase and decrease with BL, respectively (Domenici 2001). The preferred prey of Steller sea lions is small schooling fishes (Trites and Donnelly 2003), which have a significantly lower turning radius and higher rate of turn than Steller sea lions (Blake and Chan 2006). It is likely that the schooling behavior of these fishes enhances the directionality and coordination of escape when subject to predation (Domenici and Batty 1997). However, higher absolute speed and behaviors such as concentrating, disturbing, and disorienting prey could function to reduce the relative maneuverability of predator and prey.

The form of otariids (highly mobile control surfaces placed at the center of gravity, rounded cross-section, slightly dorso-ventrally compressed hips and head, flexible body, no median fins) results in superior maneuvering capabilities relative to cetaceans (Fish *et al*. 2003; Fig. 7). Yet, both otariids and cetaceans perform less well than many fish (Fig. 7). Arguably cetaceans and otariids perform less well in lateral turns than fish because of a lack of lateral compression and a principle plane of backbone flexure that is dorsal-ventral. Nevertheless, Steller sea lions are among the most maneuverable marine mammals in terms of turning radii in relation to swimming speed.

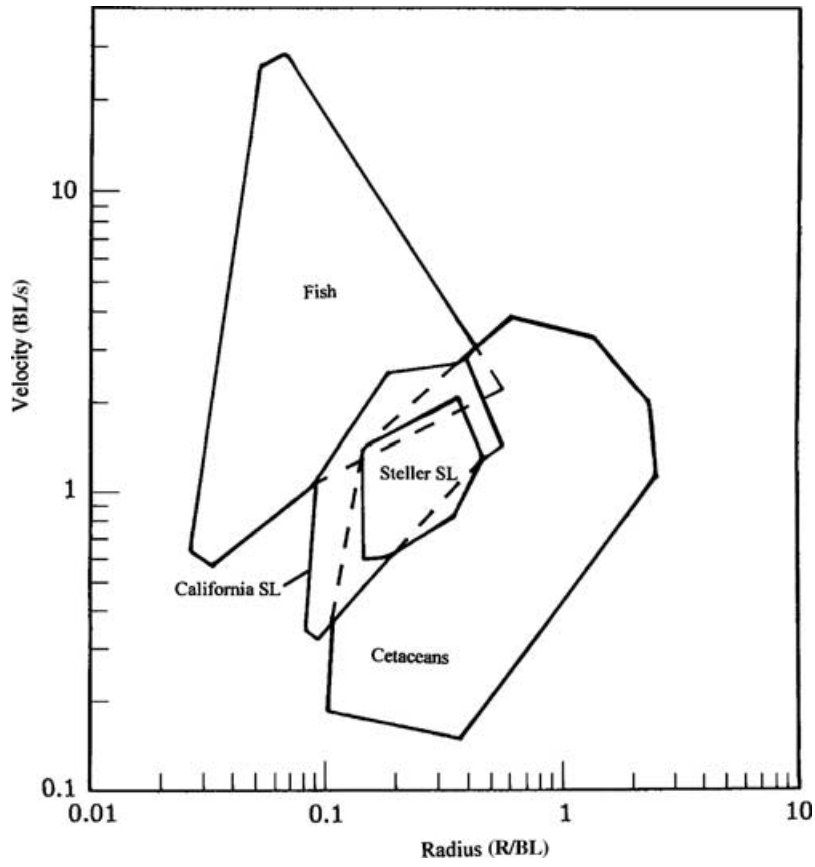


*Figure 7.* Turning speed (body length/s) *versus* normalized turning radius (turning radius/body length) of three Steller sea lions in comparison to California sea lions, cetaceans, Fish *et al*. (2003), and fish (boxfish *Ostracion meleagris*, dolphinfish *Coryphaena hippurus*, yellowtail *Ocyurus chrysurus*, yellowfin tuna *Thunnus albacares*, knifefish *Xenomystus nigri*, pike *Esox lucius*, rainbow trout *Oncorhynchus mykiss*, smallmouth bass *Micropterus dolomieu*, and angelfish *Pterophyllum eimekei*).

## LITERATURE CITED

BLAKE, R. W. 1977. On ostraciiform locomotion. Journal of the Marine Biological Association of United Kingdom 57:1047–1055.

BLAKE, R. W. 2004. Fish functional design and swimming performance. Journal of Fish Biology 65:1193–1222.

BLAKE, R. W., AND K. H. S. CHAN. in press. Models of turning dynamics and fast-start swimming of aquatic vertebrates. Journal of Fish Biology.

BLAKE, R. W., L. M. CHATTER AND P. DOMENICI. 1995. Turning radius of yellowfin tuna (*Thunnus albacares*) in unsteady swimming manoeuvres. Journal of Fish Biology 46:536–538.

CHENEVAL, O. 2005. Biomechanics of turning maneuvers in Steller sea lions (*Eumatopias jubatus*). Unpublished M. Sc. Thesis. University of British Columbia.

DOMENICI, P. 2001. The scaling of locomotor performance in predator–prey encounters: From fish to killer whales. Comparative Biochemistry and Physiology Part A: 169–182.

DOMENICI, P., AND R. S. BATTY. 1997. The escape behaviour of solitary herring (*Clupea harengus* L.) and comparisons with schooling individuals. Marine Biology 128:29–38.

DOMENICI, P., AND R. W. BLAKE. 1993. Escape trajectories in angelfish (*Pterophyllum eimekei*). Journal of Experimental Biology 177:253–272.

DOMENICI, P., E. M. STANDEN AND R. P. LEVINE. 2004. Escape manoeuvres in the spiny dogfish (*Squalus acanthias*). Journal of Experimental Biology 207:2339–2349.

DOMNING, D. P., AND V. DE BUFFRENIL. 1991. Hydrostasis in the sirenia: Quantitative data and functional interpretations. Marine Mammal Science 7:331–368.

ENGLISH, A. W. 1976. Limb movements and locomotor function in the California sea lion (*Zalophus californianus*). Journal of Zoology (London) 178:341–364.

FELDKAMP, S. D. 1987a. Foreflipper propulsion in the California sea lion, *Zalophus californianus*. Journal of Zoology (London) 212:43–57.

FELDKAMP, S. D. 1987b. Swimming in the California sea lion: Morphometrics, drag and energetics. Journal of Experimental Biology 131:117–135.

FISH, F. E. 1993. Influence of hydrodynamic design and propulsive mode on mammalian swimming energetics. Australian Journal of Zoology 42:79–101.

FISH, F. E. 1997. Biological designs for enhanced maneuverability: Analysis of marine mammal performance. *In* A. A. Onr, ed. Tenth International Symposium on Unmanned Untethered Submersible Technology: Special Session on Bio-engineering Research Related to Autonomous Underwater Vehicles. Durham.

FISH, F. E. 2002. Balancing requirements for stability and maneuverability in cetaceans. Integrative and Comparative Biology 42:85–93.

FISH, F. E., S. INNES AND K. RONALD. 1988. Kinematics and estimated thrust production of swimming harp and ringed seals. Journal of Experimental Biology 137:157–173.

FISH, F. E., J. HURLEY AND D. P. COSTA. 2003. Maneuverability by the sea lion *Zalophus californianus*: Turning performance of an unstable body design. Journal of Experimental Biology 206:667–674.

GODFREY, S. J. 1985. Additional observations of subaqueous locomotion in California sea lion (*Zalophus californianus*). Aquatic Mammals 11:53–57.

HOWLAND, H. C. 1974. Optimal strategies for predator avoidance: the relative importance of speed and maneuverability. Journal of Theoretical Biology 47:333–350.

HUGHES, N. F., AND L. H. KELLY. 1996. A hydrodynamic model for estimating the energetic cost of swimming maneuvers from a description of their geometry and dynamics. Canadian Journal of Fisheries and Aquatic Sciences 53:2484–2493.

LOUGHLIN, T. R., M. A. PEREZ AND R. L. MERRICK. 1987. Eumetopias jubatus. Pages 1–7 *in* B. J. Verts and S. Anderson, Mammalian species account no. 283. The American Society of Mammalogists.

MARESH, J. L., F. E. FISH, D. P. NOWACEK, S. M. NOWACEK AND R. S. WELLS. 2004. High performance turning capabilities during foraging by bottlenose dolphins (*Tursiops truncatus*). Marine Mammal Science 20:498–509.

MERRICK, R. L., M. K. CHUMBLEY AND G. V. BYRD. 1997. Diet diversity of Steller sea lions (*Eumetopias jubatus*) and their population decline in Alaska: A potential relationship. Canadian Journal of Fisheries and Aquatic Sciences 54:1342–1348.

NOWACEK, D. P. 2002. Sequential foraging behaviour of bottlenose dolphins, *Tursiops truncatus*, in Sarasota Bay, Fl. Behaviour 139:1125–1145.

PONGANIS, P. J., E. P. PONGANIS, K. V. PONGANIS, G. L. KOOYMAN, R. L. GENTRY AND F. TRILLMICH. 1990. Swimming velocities in otariids. Canadian Journal of Zoology 68:2105–2112.

RIEDMAN, M. 1990. The pinnipeds: Seals, sea lions, and walruses. University of California Press, Berkeley, CA.

ROSEN, D. A. S., AND A. W. TRITES. 2004. Satiation and compensation for short-term changes in food quality and availability in young Steller sea lions (*Eumetopias jubatus*). Canadian Journal of Zoology 82:1061–1069.

SINCLAIR, E. H., AND T. K. ZEPPELIN. 2002. Seasonal and spatial differences in diet in the western stock of Steller sea lions (*Eumetopias jubatus*). Journal of Morphology 83:973–990.

STELLE, L. L., R. W. BLAKE AND A. W. TRITES. 2000. Hydrodynamic drag in Steller sea lions (*Eumetopias jubatus*). Journal of Experimental Biology 203:1915–1923.

TRITES, A. W., AND C. P. DONNELLY. 2003. The decline of Steller sea lions *Eumetopias jubatus* in Alaska: A review of the nutritional stress hypothesis. Mammal Review 33:3–28.

WALKER, J. A. 2000. Does a rigid body limit maneuverability? Journal of Experimental Biology 203:3391–3396.

WEBB, P. W. 1991. Composition and mechanics of routine swimming of rainbow trout, *Oncorhynchus mykiss*. Canadian Journal of Fisheries of Aquatic Sciences 48:583–590.

WEIHS, D. 2002. Stability versus maneuverability in aquatic locomotion. Integrative and Comparative Biology 42:127–134.

WILLIAMS, T. M., AND G. L. KOOYMAN. 1985. Swimming performance and hydrodynamic characteristics of harbor seals *Phoca vitulina*. Physiological Zoology 58:576–589.

WINSHIP, A. J., A. W. TRITES AND D. G. CALKINS. 2001. Growth in body size of the Steller sea lion. Journal of Mammology 82:500–519.

Received: 19 October 2005
Accepted: 20 August 2006